Phase Structure of the Exact Graft Copolymer Synthesized by Iterative Methodology Based on Living Anionic Polymerization

Yu-Hsuan Lin, Hsin-Lung Chen,* Raita Goseki, Akira Hirao

Exact graft copolymer (EGC) is a type of copolymer with precisely defined molecular parameters, including the number of grafts per molecule (n), the length of the grafts (l_g), and the separation distance between the junction points (ε) in the backbone. In the present study, the phase structure of the EGC composed of poly(2-vinyl pyridine) backbone and polystyrene graft with $n = 2$ and $n = 3$ under fixed ε and l_g is systematically investigated to seek a general understanding on the effect of the graft architecture on the domain spacing of the microphase-separated structure and the order–disorder transition temperature (T_{ODT}). It is found that the T_{ODT} associated with the fluctuation-induced ODT of the EGC increases with increasing n due to the increase of the total molecular weight. Nevertheless, the domain spacing does not exhibit a monotonic change with n, as the EGC with $n = 2$ shows the largest domain spacing compared with that of EGC with $n = 3$ and the corresponding linear diblock copolymer. The experimental observation on the domain spacing is explained by a thermodynamic model considering the packing mode of the constituting chains under the junction constraint.

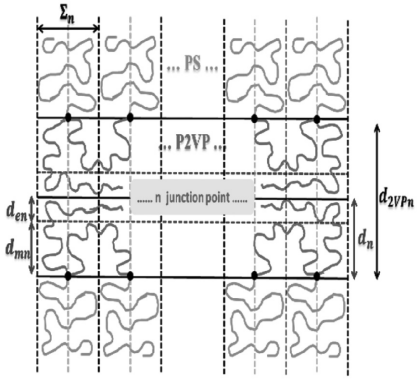

1. Introduction

Polymer molecules composed of multiple building blocks undergo microphase separation once the repulsion among the building blocks is sufficiently strong. The most representative system is the linear block copolymers (bcp) consisting of chemically different block chains interconnected at their ends. The microphase separation between the constituent blocks of bcp may lead to a series of long-range ordered nanostructures,[1–3] including one-dimensionally stacked lamellae, hexagonally packed cylinders, body-centered cubic (BCC) packed spheres, and double gyroid.[4] The morphology formed is governed by the constituent volume fraction (f) and the segregation strength represented by the product of the Flory–Huggins interaction parameter (χ) and the overall degree of polymerization (N). The plot of χN versus f constructs the universal phase diagram defining the spinodal lines separating ordered and disordered state of the bcp.[1,5–8] In terms of the free energy contributions, the phase behavior of bcp is dedicated mainly by the interplay between the interfacial free energy and the conformational entropy loss associated with the stretching of the block chains in the ordered state under the constraint of melt incompressibility.[4,7]

Besides linear bcps, the advancement of anionic polymerization has led to the precise synthesis of the copolymers with well-defined nonlinear architecture, such as miktoarm, block arm, and graft copolymer. It is

Y.-H. Lin, Prof. H.-L. Chen
Department of Chemical Engineering
National Tsing Hua University
Hsinchu 30013, Taiwan
E-mail: hlchen@che.nthu.edu.tw
Prof. R. Goseki, Prof. A. Hirao
Department of Organic and Polymeric Materials
Tokyo Institute of Technology
Ohokayama, Meguro-ku, Tokyo 152-8552, Japan

© 2017 WILEY-VCH Verlag GmbH & Co. KGaA, Weinheim

DOI: 10.1002/macp.201700150

conceivable that the nonlinear architecture may modify the free energy components, thereby perturbing the phase behavior of the nonlinear copolymer relative to that of the corresponding linear bcp, as has been demonstrated both theoretically and experimentally.[9–14] The present study is focused on the phase structure of the graft copolymer with exactly controlled architecture. Graft copolymer is composed of a backbone grafted with chemically different side chains. Its molecular architecture is characterized by four parameters, namely, the length or molecular weight of the backbone, the length of the graft chain (l_g), the separation distance between the junction points in the backbone (ε), and the number of junction points or grafts per molecule (n).[15–17] The complex combination of these molecular parameters may result in a broad spectrum of phase behavior which deviates greatly from that of the linear bcp in terms of the domain spacing and the phase boundaries associated with the order–order and order–disorder transition.

The synthesis of the graft copolymer with exact control of the molecular parameters was not realized until 2000 when Hadjichristidis and Paraskeva successfully synthesized a graft copolymer composed of polyisoprene (PI) backbone and two polystyrene (PS) graft chains using a stepwise iterative methodology.[18] Hirao et al. later extended this iterative concept to synthesize the graft copolymers composed of poly(2-vinyl pyridine) (P2VP) backbone and PS grafts with precisely defined molecular parameters. The graft copolymers thus synthesized are specifically called "exact graft copolymer (EGC)" to distinguish from the system without rigorous architectural control.[15–18] The availability of the EGC samples provides the mean to examine the phase structure of graft copolymer for unambiguous comparison with that of the linear bcp to resolve the molecular architecture effect on the self-assembly behavior of copolymers in detail. In this study, we investigate the phase behavior of the EGC composed of P2VP backbone and PS grafts (denoted as "EG(P2VP-PS)$_n$") synthesized by the anionic polymerization using iterative approach.[15–17] The copolymers possess different numbers of junction points of PS graft per molecule under fixed graft length and length between the junction points. Here we concentrate specifically on the domain spacing (D) and order–disorder transition (ODT) of the lamellae-forming EGCs, as compared to those of the corresponding linear diblock, PS-*b*-P2VP bearing the same block lengths to establish a deeper understanding on the phase structure of graft copolymer. To interpret the molecular architecture effect on D, we further develop a thermodynamic model which is able to predict the variation of D with n for EGC.

2. Experimental Section

2.1. Materials and Sample Preparation

The synthetic scheme of the EGC, EG(P2VP-PS)$_n$, is shown in Scheme 1 and its detailed procedure is described as follows.

2.1.1. Synthesis of In-Chain-SiOP-Functionalized PS-*b*-P2VP

Under high vacuum conditions, styrene (5.74 mmol) in tetrahydrofuran (THF) (5.6 mL) solution was precooled at –78 °C was

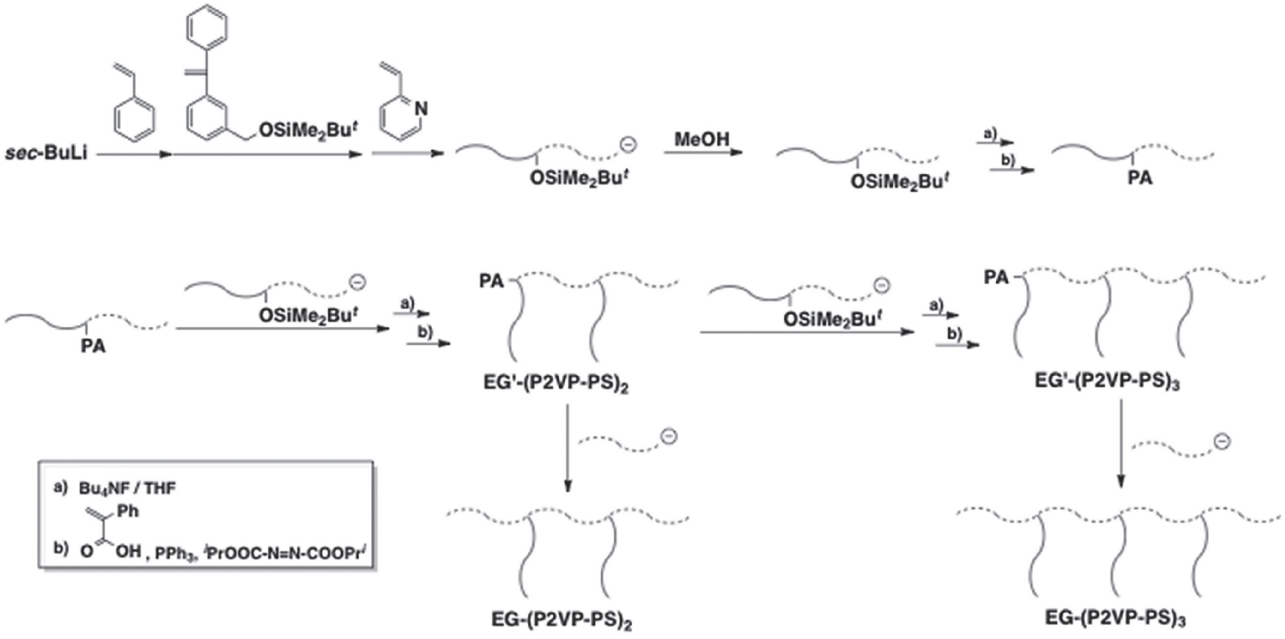

Scheme 1. Synthetic scheme of the exact graft copolymer (EG(P2VP-PS)$_n$).

© 2017 WILEY-VCH Verlag GmbH & Co. KGaA, Weinheim
ADVANCED SCIENCE NEWS
www.advancedsciencenews.com

added at once with shaking to *sec*-BuLi (0.125 mmol) in heptane solution at −78 °C, and the polymerization was allowed to stand for 20 min. Then, 1-(3-*tert*-butyldimethylsilyloxymethylphenyl)-1-phenyl ethylene (0.225 mmol) in THF (2.37 mL) solution was precooled to −78 °C and then carefully added to a polymer solution at −78 °C for 30 min. After a small amount of aliquot of the ω-chain-end-SiOP-functionalized PSLi was taken for the characterization, 2-vinylpyridine (6.19 mmol) in THF (6.0 mL) precooled at −78 °C was added with vigorous shaking to polymerize for 1 h. The polymerization was quenched with a few drops of degassed methanol. The polymer solution was concentrated and poured into a large excess of hexanes to precipitate the polymer. The resulting polymer was further purified by reprecipitation twice from THF solution into hexane and freeze-dried from its absolute benzene solution for 24 h (1.05 g, 84%). The resulting in-chain-SiOP-functionalized PS-*b*-P2VP was characterized by size exclusion chromatography (SEC) and ^{1}H NMR. $M_{n\text{RALLS}}$ = 9900, M_w/M_n = 1.03. ^{1}H NMR (300 MHz): δ = 8.51–8.05 (broad, N=CH), 7.55–6.12 (broad, Ar), 4.45 (s, Ph−CH_2−O−Si), 2.47–1.32 (broad, main chain), 0.84 (s, C(CH_3)$_3$), −0.03 (s, Si(CH_3)$_2$).

2.1.2. Synthesis of In-Chain-α-phenylacrylate (PA) Functionalized PS-*b*-P2VP

Under a nitrogen atmosphere, the in-chain-SiOP-functionalized PS-*b*-P2VP (M_n = 9 900, 1.02 g, 0.103 mmol for SiOP terminus) was treated with Bu_4NF (1.00 mmol) in THF (1.00 mL) at 0 °C for 9 h in order to remove the silyl protective group of the SiOP terminus. After quenching the reaction with a small amount of methanol and removing the solvent, the polymer dissolved in THF was poured into a large excess of hexane to precipitate. The resulting in-chain-hydroxyl PS-*b*-P2VP was freeze-dried from its absolute benzene solution for 24 h under vacuum. The yield of the polymer was 92% yield (0.93 g, 0.0949 mmol). $M_{n\text{RALLS}}$ = 9800, M_w/M_n = 1.04. ^{1}H NMR (300 MHz): δ = 8.56–8.04 (broad, N=CH), 7.58–6.18 (broad, Ar), 4.46 (s, Ph−CH2−OH), 2.44–1.31 (broad, main chain).

The in-chain-hydroxyl PS-*b*-P2VP (M_n = 9800, 0.92 g, 0.0929 mmol for hydroxyl terminus), α-phenylacrylic acid (0.21 g, 1.42 mmol), and PPh_3 (0.32 g, 1.17 mmol) were dissolved in THF (10 mL) and diisopropylazodicarboxylate (DIAD, 0.54 g, 0.54 mmol) was added dropwise at 0 °C, and the reaction mixture was allowed to stir at room temperature for 24 h. After quenching the reaction with a small amount of methanol and removing the solvent, the polymer dissolved in THF was poured into a large excess of hexanes to precipitate. The resulting polymer was purified by column chromatography with hexane/dichloromethane (50/50). Finally, the PA-functionalized PS-*b*-P2VP was freeze-dried from its absolute benzene solution for 48 h under vacuum (0.79 g, 0.0797 mmol, 85%). $M_{n\text{RALLS}}$ = 9900, M_w/M_n = 1.03. ^{1}H NMR (300 MHz): δ = 8.51–8.06 (broad, N=CH), 7.51–6.09 (broad, Ar), 5.81 (d, C=CH2), 4.98 (s, Ph−CH2−O−(C=O)), 2.49–1.40 (broad, main chain).

2.1.3. General Procedure for Synthesis of a Series of Exact graft $(AB)_n$ Copolymers Composed of PS and P2VP (EG′(P2VP-PS)$_n$)

Starting from the in-chain-PA-functionalized PS-*b*-P2VP above synthesized, a series of EG′(P2VP-PS)$_n$ polymers (n = 2 and 3) was synthesized by repeating the same iterative synthetic sequence. Details of the preparation of the in-chain-SiOP-functionalized living PS-*b*-P2VP anion and the in-chain modification reactions to PA function via the SiOP terminus were described above. In the final linking reaction, an excess of in-chain-SiOP-functionalized PS-*b*-P2VP anion was reacted with in-chain-PA-functionalized block copolymer at −78 °C for 24 h. The molar ratio of diblock copolymer anion to the PA-functionalized block copolymer increases from 1.5 to 3.5 as the iteration proceeded. After quenching the reaction with a small amount of degassed methanol, the reaction mixture was poured into a large excess of hexane to precipitate the polymers. SEC curves of the crude compounds always showed only two peaks corresponding to the objective exact-graft copolymer and the deactivated diblock copolymer anion used in excess. The objective polymer was isolated by SEC fractionation. The isolated polymer was reprecipitated from THF solution to hexane twice, and freeze-dried from its absolute benzene solution for 48 h. The resulting in-chain-functionalized exact-graft polymers were characterized by SEC, RALLS, and ^{1}H NMR in order to determine the absolute molecular weights, molecular weight distributions, composition ratios, and degree of SiOP-functionalities.

2.1.4. Synthesis of Exact Graft (P2VP-PS)$_2$ and (P2VP-PS)$_3$ Copolymers Composed of PS and P2VP (EG(PS-P2VP)$_n$)

The SiOP-functionalized living PS-*b*-P2VP anion (M_n = 10 300) was prepared by the sequential block copolymerization of 2VP (5.57 mmol) in THF (5.14 mL) with ω-chain-end-SiOP-functionalized PSLi (M_n = 5300, 0.116 mmol, ω-chain-end-capped with DPE) in THF (5.89 mL) at −78 °C for 1 h. To this polymer solution, a THF solution (10.3 mL) of the in-chain-PA-functionalized PS-*b*-P2VP (M_n = 9900, 0.78 g, 0.0787 mmol for PA moiety) precooled at −78 °C was carefully added and the reaction mixture was allowed to stand at −78 °C for 24 h. The reaction was terminated with degassed methanol. After usual work-up, an EG′(P2VP-PS)$_2$ was isolated in 41% yield by SEC fractionation, reprecipitated from THF solution to hexane mixture, and freeze-dried from its absolute benzene solution. $M_{n\text{RALLS}}$ = 20 100, M_w/M_n = 1.03. ^{1}H NMR (300 MHz): 8.50–8.06 (broad, N=CH), 7.54–6.10 (broad, Ar), 4.45 (s, Ph−CH2−O−Si), 2.49–1.31 (broad, main chain), 0.82 (s, C(CH_3)$_3$), −0.01 (s, Si(CH_3)$_2$).

The SiOP-functionalized EG′(P2VP-PS)$_2$ (M_n = 20 100, 0.65 g, 0.0323 mmol for SiOP group) was carefully treated with Bu_4NF (1.01 mmol) in THF (10 mL) at 0 °C for 9 h. The hydroxyl-terminated EG′(P2VP-PS)$_2$ was obtained in 94% yield (0.61 g, 0.0303 mmol). $M_{n\text{RALLS}}$ = 20 000, M_w/M_n = 1.03. The hydroxyl-terminated EG′(P2VP-PS)$_2$ (M_n = 20 000, 0.61 g, 0.0303 mmol for hydroxyl terminus), α-phenylacrylic acid (0.07 g, 0.47 mmol), and PPh_3 (0.11 g, 0.39 mmol) were dissolved in THF (10 mL) and DIAD (0.18 g, 0.18 mmol) was added slowly at 0 °C and the reaction mixture was allowed to stir at room temperature for 24 h under a nitrogen atmosphere.

After the usual workup procedure mentioned above, the PA-terminated EG′(P2VP-PS)$_2$ was obtained in 89% yield (0.542 g, 0.0270 mmol for PA function). $M_{n\text{RALLS}}$ = 20 100, M_w/M_n = 1.03. The exact graft copolymer composed of a P2VP backbone and two PS chains (EG(P2VP-PS)$_2$) was synthesized by performing the linking reaction between living P2VP (M_n = 5200, 0.0153 mmol) and the PA-terminated EG′(P2VP-PS)$_2$ (0.202 g, 0.0100 mmol). The

© 2017 WILEY-VCH Verlag GmbH & Co. KGaA, Weinheim

Table 1. Characterization results of the molecular weights and compositions of the copolymers synthesized.

Code	$M_n \times 10^{-3}$ [g mol^{-1}]			M_w/M_n [a]	PS/P2VP [w/w]	
	Calcd.	SEC[a]	SEC-LS[b]		Calcd.	^{1}H NMR[c]
PS-*b*-P2VP	9.99	9.80	9.88	1.03	49/51	50/50
EG′(P2VP-PS)$_2$	20.2	19.6	20.1	1.03	51/49	51/49
EG(P2VP-PS)$_2$	25.4	21.9	25.2	1.04	44/56	45/55
EG′(P2VP-PS)$_3$	31.2	26.7	30.5	1.04	48/52	50/50
EG(P2VP-PS)$_3$	35.9	29.7	35.2	1.04	45/55	44/56

[a]Estimated by SEC with standard polystyrenes; [b]Determined by SEC equipped with triple detectors; [c]Determined by ^{1}H NMR.

target polymer was isolated by SEC fractionation in 52% yield (0.132 g, 0.00523 mmol). $M_{n\text{RALLS}}$ = 25 200, M_w/M_n = 1.04. ^{1}H NMR (300 MHz): δ = 8.51–8.06 (broad, N=CH), 7.55–6.12 (broad, Ar), 5.09–4.39 (m, Ph−CH2−O−(C=O)), 2.48–1.31 (broad, main chain).

The exact graft copolymer precursor having three PS graft chains (EG′(P2VP-PS)$_3$) was synthesized by performing the linking reaction between a living in-chain-SiOP-functionalized PS-*b*-P2VP (M_n = 11 000, 0.034 mmol) was used in a 2.0-fold molar excess for the PA function (0.342 g, 0.017 mmol). The target polymer was isolated by SEC fractionation in 54% yield (0.259 g). $M_{n\text{RALLS}}$ = 30 500, M_w/M_n = 1.04. The resulting polymer obtained as above was treated with Bu_4NF, followed by the Mitsunobu esterification reaction with α-phenylacrylic acid, to transform the SiOP group into PA function. Then, a living P2VP (M_n = 5400, 0.0103 mmol) was reacted with the PA-functionalized EG′(P2VP-PS)$_3$ (0.169 g, 0.00558 mmol). The resulting polymer was isolated in 51% yield by SEC fractionation (0.101 g). $M_{n\text{ RALLS}}$ = 35 200, M_w/M_n = 1.04. ^{1}H NMR (300 MHz): δ = 8.40–8.10 (broad, N=CH), 7.52–6.14 (broad, Ar), 5.08–4.37 (m, Ph−CH2−O−(C=O)), 2.51–1.38 (broad, main chain).

Table 1 shows the characterization results of the molecular weights and compositions of the copolymers synthesized. The diblock copolymer PS-*b*-P2VP and the EGC, EG(P2VP-PS)$_2$ and EG(P2VP-PS)$_3$, were chosen for the further study of their phase structures. Table 2 lists the molecular characteristics of these three samples, including the molecular weights and the volume fractions of the PS and P2VP blocks. For the sake of simplicity, EG(P2VP-PS)$_2$ and EG(P2VP-PS)$_3$ were hereafter denoted as EG2 and EG3, respectively. It can be seen that all copolymers bore almost the same lengths of PS and P2VP blocks, where the term "block" denotes the PS and P2VP chains constituting PS-*b*-P2VP,

Table 2. Molecular characteristics of the three copolymer samples studied.

Code	M_n of PS block in copolymer [g mole^{-1}]	M_n of P2VP block in copolymer [g mole^{-1}]	f_{PS}
PS-*b*-P2VP	4900	5100	0.47
EG2	5590	4740	0.42
EG3	5360	4940	0.43

the P2VP chains between the junction points in the backbone and the PS grafts in the EGC.

The powders of the copolymer samples were dissolved in THF to obtain a homogeneous solution by stirring at 45 °C for 1 h. The solutions were poured onto the petri dishes followed by evaporating most solvent at room temperature for 24 h. The films were then dried in vacuum at 70 °C for 72 h to remove the residual solvent.

2.2. Small Angle X-ray Scattering (SAXS) Measurement

The temperature-dependent SAXS measurements were performed at Beamline 23A1 of the National Synchrotron Radiation Research Center, Hsinchu, Taiwan. The sample-to-detector distance was 3380.1 mm and the energy of X-ray source was 15 keV which prescribed the scattering vector q range of 0.05–4.0 nm^{-1}. The scattering signals were recorded by the 2D MarCCD detector with a resolution of 512 × 512 pixels. The magnitude of the scattering vector is given by $q=\frac{4\pi}{\lambda}\sin\left(\frac{\theta}{2}\right)$, with θ and λ being the scattering angle and X-ray-wavelength, respectively. The scattering intensity profile was output as the plot of the scattering intensity (I) versus the q after corrections for transmission of air and background. For the temperature-dependent SAXS study, the sample was equilibrated at each temperature for 5 min followed by data acquisition for 5 min.

3. Results and Discussion

3.1. Temperature-Dependent SAXS Results of PS-*b*-P2VP and EGCs

Figure 1a displays the temperature-dependent SAXS profiles of PS-*b*-P2VP collected in a heating cycle. The SAXS profile at 30 °C displayed a strong and sharp primary peak at 0.50 nm^{-1}, indicating the occurrence of microphase separation in the diblock. Judging from the symmetric composition (f_{2VP} = 0.53) of the copolymer, the expected microphase-separated structure was 1D stacked lamellae with the domain spacing of 12.64 nm. The symmetric composition suppresses the second-order peak associated with the lamellar structure in the SAXS profile.[19]

It can be seen in Figure 1a that the primary peak diminished in intensity with increasing temperature clearly above 110 °C, implying the occurrence of ODT. The inverse of the peak intensity (I_m^{-1}) was plotted against the inverse of absolute temperature to identify the T_{ODT}, as shown in Figure 1b. A small discontinuity in the plot was observed at 117.3 °C, which defines the T_{ODT} associated with the fluctuation-induced ODT from the lamellar structure to the disordered state characterized by the spinodal-like composition fluctuations.[2,20]

© 2017 WILEY-VCH Verlag GmbH & Co. KGaA, Weinheim

ADVANCED SCIENCE NEWS
www.advancedsciencenews.com

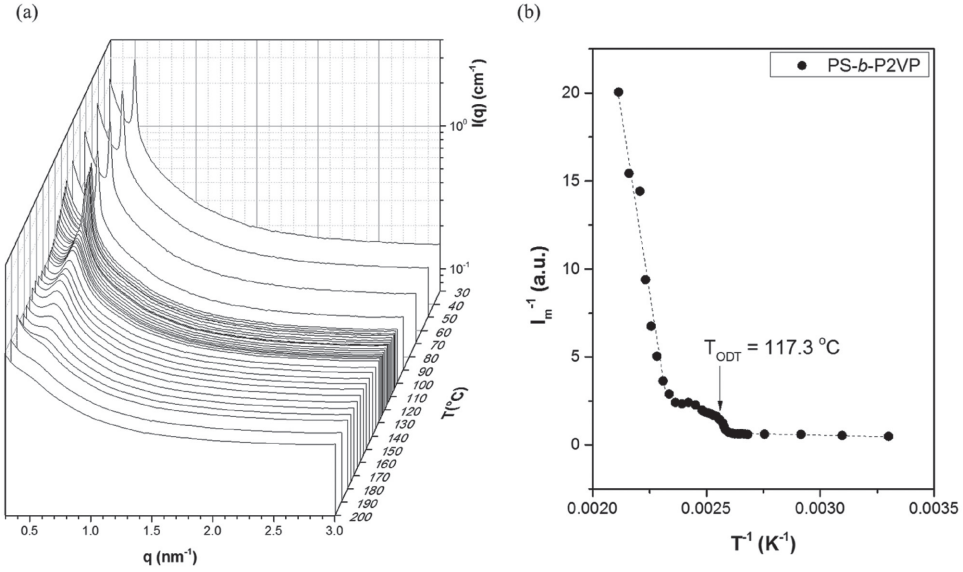

Figure 1. a) The temperature-dependent SAXS profiles of PS-*b*-P2VP collected in a heating cycle from 30 to 200 °C. b) I_m^{-1} versus T^{-1} plot of PS-*b*-P2VP for the determination of T_{ODT}.

According to the Helfand–Fredrickson theory,[20,21] such an ODT is a weak first-order transition characterized by a small discontinuous change in scattering peak intensity across the ODT. Increasing temperature suppresses the amplitude of the spinodal-like composition fluctuations in the disordered state, and the mean-field disordered state in which the copolymer is in a fully single phase may be accessed when the temperature is sufficiently high.[1,22]

Figure 2a shows the temperature-dependent SAXS profiles of EG2 collected in a heating cycle from 30 to 200 °C. The SAXS curve at 30 °C exhibited a sharp peak at 0.46 nm^{-1}, which was attributed to the first-order diffraction maximum associated with the lamellar structure formed by the microphase separation between P2VP backbone and PS grafts. The lamellar morphology was confirmed by the TEM micrograph displayed in the Supporting Information. The second-order peak was again indiscernible due to the symmetric composition. The domain spacing of EG2 at 30 °C calculated from the primary peak position was 13.7 nm, which was about 1 nm thicker than that of the corresponding PS-*b*-P2VP.

As can be seen in Figure 2a, the primary peak diminished and broadened progressively with increasing

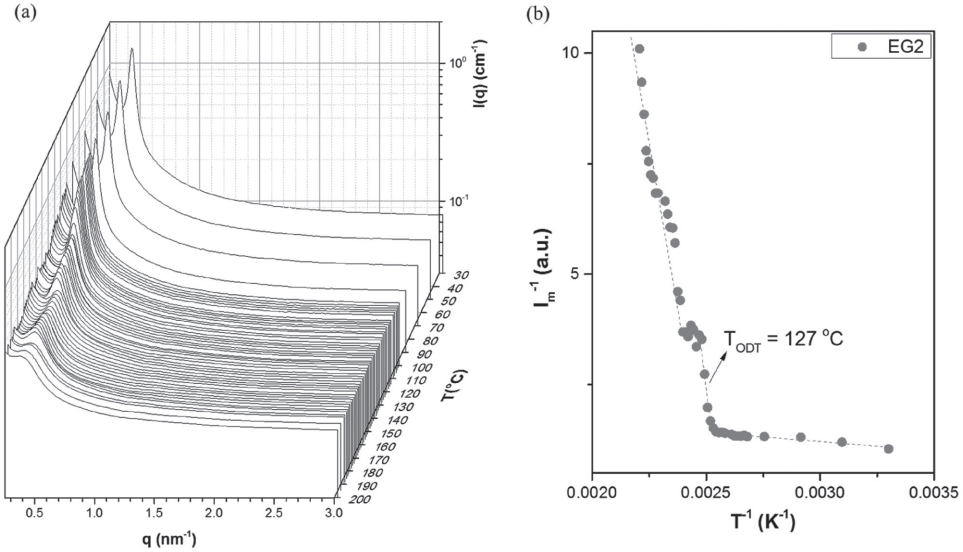

Figure 2. a) The temperature-dependent SAXS profiles of EG2 collected in a heating cycle from 30 to 200 °C. b) I_m^{-1} versus T^{-1} plot of EG2 for the determination of T_{ODT}.

© 2017 WILEY-VCH Verlag GmbH & Co. KGaA, Weinheim

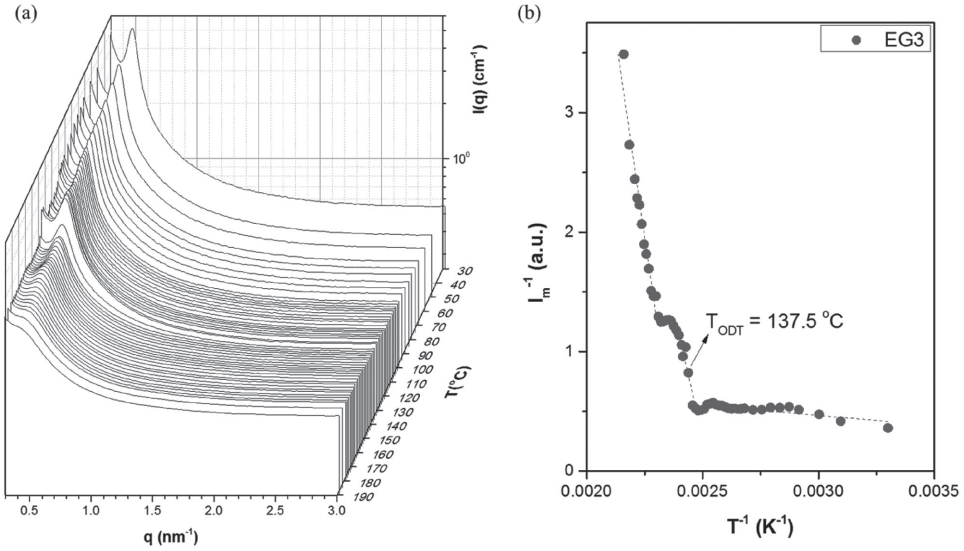

Figure 3. a) The temperature-dependent SAXS profiles of EG3 collected in a heating cycle from 30 to 190 °C. b) I_m^{-1} versus T^{-1} plot of EG3 for the determination of T_{ODT}.

temperature. The plot of I_m^{-1} versus T^{-1} as shown in Figure 2b revealed weak discontinuity, signaling that the fluctuation effect on ODT was also operative in EGC. The T_{ODT} thus determined was 127 °C. The T_{ODT} of EG2 was higher than that of PS-*b*-P2VP.

The temperature-dependent SAXS profiles of EG3 are displayed in Figure 3a. The strong primary peak observed at 30 °C attested the occurrence of microphase separation but the peak was broader than that of PS-*b*-P2VP, implying that the long-range order of the lamellar structure formed in the EGC was poorer. The domain spacing at 30 °C was 13.1 nm. The I_m^{-1} versus T^{-1} plot of EG3 shown in Figure 3b yielded the T_{ODT} of EG3 of 137.5 °C.

Table 3 summarizes the T_{ODT}s of the three copolymers. All three samples exhibited a weak first-order transition corresponding to the transition from the ordered state to the fluctuation-induced disordered state, the T_{ODT} followed the order of EG3 > EG2 > PS-*b*-P2VP.

Figure 4 displays the temperature variations of the domain spacings (D) of PS-*b*-P2VP and the two EGCs. The values of D remained virtually unperturbed below ≈100 °C, because both PS and P2VP were in the glassy state ($T_g^{PS} \approx 100$ °C, $T_g^{P2VP} \approx 95$ °C). The domain spacing underwent an abrupt drop right above T_g, which may be attributed to the relaxation of the nonequilibrium structure arrested into the glassy state upon solvent casting. In the cases of EG2 and EG3, the domain spacing experienced another steep drop as the fluctuation-induced disordered state was accessed. It is noted that D calculated from the scattering peak maximum at $T > T_{ODT}$ corresponds to the characteristic wavelength of the composition fluctuation.[20] Now we direct the attention to the architecture effect on the domain spacing in the ordered state. It can be seen from Figure 4, that the domain spacings of the copolymers studied followed the order of D(EG2) > D(EG3) > D(PS-*b*-P2VP). Later, we will formulate a thermodynamic model for the domain spacing to describe the effect of the number of graft per molecule on D.

Table 3. T_{ODT}'s of the copolymers studied.

Sample	T_{ODT} [°C]
PS-*b*-P2VP	117.3
EG2	127.0
EG3	137.5

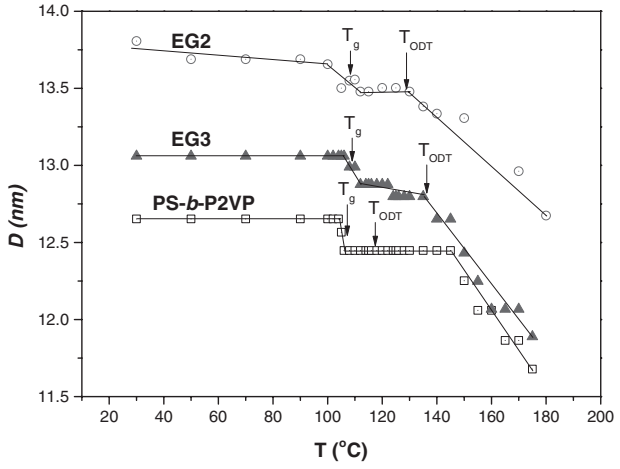

Figure 4. Temperature variations of the domain spacings of PS-*b*-P2VP and EGCs.

Macromol. Chem. Phys. **2017**, *218*, 1700150
© 2017 WILEY-VCH Verlag GmbH & Co. KGaA, Weinheim

ADVANCED SCIENCE NEWS
www.advancedsciencenews.com

3.2. Thermodynamic Model for the Domain Spacing of Exact Graft Copolymer

Our SAXS results have shown that the domain spacing depended on n, where D followed the order of EG2 > EG3 > PS-*b*-P2VP, that is, the domain spacing of EGC is larger than that of the corresponding linear diblock. Here, we attempt to predict the variation of D with n using a simple thermodynamic model. Moreover, we will provide an explanation on why the domain spacing of the linear PS-*b*-P2VP was smaller than that of the EGC based on the argument of the entropic contribution to surface free energy.

Here we assume that the copolymers are in the strong segregation regime, in which the microphase-separated domains compose of pure constituents with sharp interface. Let us first consider PS-*b*-P2VP, which exhibits the lamellar structure schematically illustrated in Figure 5a. The corresponding interfacial free energy per diblock molecule is given by

$$F_{\text{int}} = \Sigma_{\text{b}}\gamma_{\text{b}} \tag{1}$$

where Σ_{b} is the cross sectional area per junction point and γ_{b} is the surface free energy of the linear diblock. Assuming bilayer arrangement in the microdomain, Σ_{b} can be expressed as

$$\Sigma_{\text{b}} = \frac{2m_{\text{PS}_{\text{b}}}}{d_{\text{PS}_{\text{b}}}\rho_{\text{PS}}} = \frac{2m_{2\text{VP}_{\text{b}}}}{d_{2\text{VP}_{\text{b}}}\rho_{2\text{VP}}} \tag{2}$$

where m_i, d_i, and ρ_i are the molecular mass, domain thickness, and mass density of block i (i = PS or P2VP), respectively. Substituting Equation (2) into Equation (1) and recognizing that $d_{2\text{VP}_{\text{b}}} = f_{2\text{VP}}D_{\text{b}}$ (with D_{b} being the domain spacing of the diblock), we have

$$F_{\text{int}} = \left(\frac{2m_{2\text{VP}_{\text{b}}}\gamma_{\text{b}}}{\rho_{2\text{VP}}f_{2\text{VP}_{\text{b}}}}\right)\frac{1}{D_{\text{b}}} \tag{3}$$

The conformational free energy is given by

$$F_{\text{conf}} = \frac{3}{2}k_{\text{B}}T\left[\frac{\left(\frac{d_{2\text{VP}_{\text{b}}}}{2}\right)^2}{N_{2\text{VP}_{\text{b}}}a_{2\text{VP}}^2} + \frac{\left(\frac{d_{\text{PS}_{\text{b}}}}{2}\right)^2}{N_{\text{PS}_{\text{b}}}a_{\text{PS}}^2}\right] = \frac{3}{8}k_{\text{B}}T\left[\frac{f_{2\text{VP}_{\text{b}}}^2}{N_{2\text{VP}_{\text{b}}}a_{2\text{VP}}^2} + \frac{f_{\text{PS}_{\text{b}}}^2}{N_{\text{PS}_{\text{b}}}a_{\text{PS}}^2}\right]D_{\text{b}}^2 \tag{4}$$

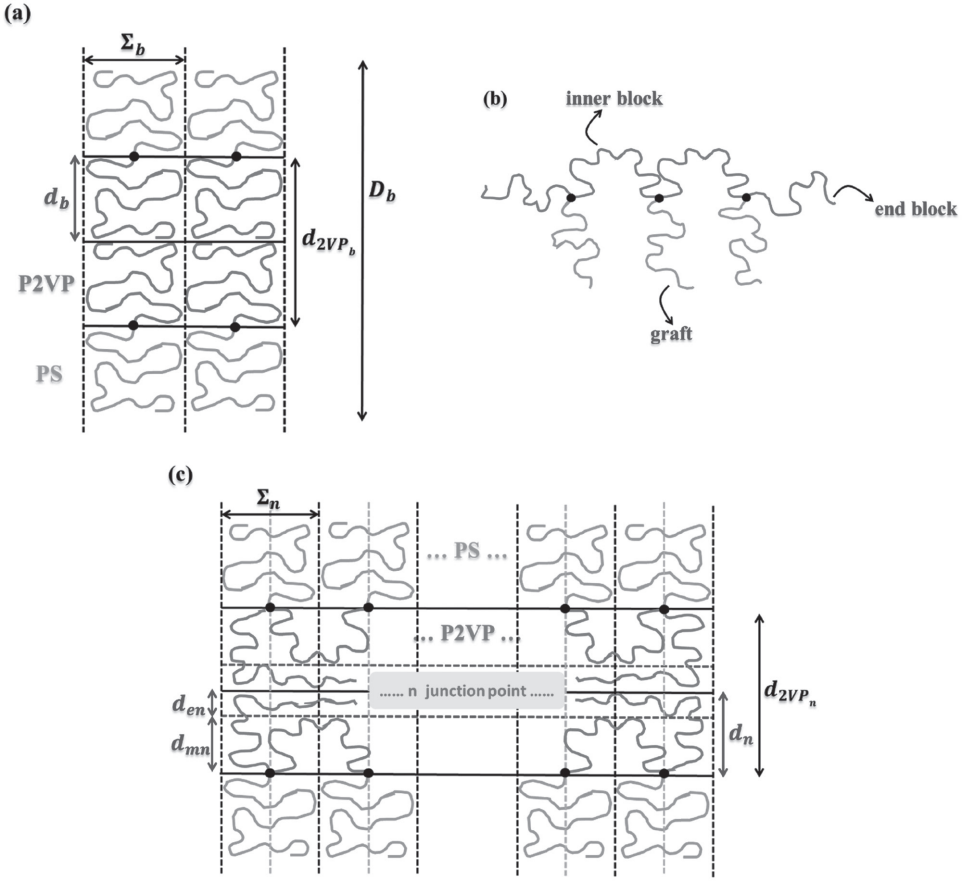

Figure 5. a) Schematic illustration of the chain packings in the lamellar domains of PS-*b*-P2VP. b) The characteristics of the block chains in EGC. c) The proposed chain packing in the lamellar microdomain of EGC.

© 2017 WILEY-VCH Verlag GmbH & Co. KGaA, Weinheim

where N_i and a_i are the number and Kuhn length of segment i constituting the block chain. The total free energy is given by the sum of F_{int} and F_{conf}, viz

$$F_{tot}=\left(\frac{2m_{2VP_b}\gamma_b}{\rho_{2VP}f_{2VP_b}}\right)\frac{1}{D_b}+\frac{3}{8}k_BT\left[\frac{f_{2VP_b}^{\ 2}}{N_{2VP_b}a_{2VP}^{\ 2}}+\frac{f_{PS_b}^{\ 2}}{N_{PS_b}a_{PS}^{\ 2}}\right]D_b^2 \quad (5)$$

The equilibrium domain spacing of the diblock, $D_{b,eq}$, is prescribed by the minimization of the total free energy with respect to D_b, i.e., $\left(\frac{\partial F_{tot}}{\partial D_b}\right)_{D_{b,eq}}=0$

Consequently, $D_{b,eq}$ is given by

$$D_{b,eq}=\left(\frac{8\gamma_b}{3k_BT}\right)^{\frac{1}{3}}\left[\frac{m_{2VP_b}}{\rho_{2VP}f_{2VP_b}\left(\frac{f_{2VP_b}^{\ 2}}{N_{2VP_b}a_{2VP}^{\ 2}}+\frac{f_{PS_b}^{\ 2}}{N_{PS_b}a_{PS}^{\ 2}}\right)}\right]^{\frac{1}{3}} \quad (6)$$

Since $m_{2VP_b}=\rho_{2VP}N_{2VP_b}a_{2VP}^{\ 3}$ and $N_{PS_b}=N_{2VP_b}\left(\frac{a_{2VP}}{a_{PS}}\right)^3\left(\frac{f_{PS_b}}{f_{2VP_b}}\right)$,

Equation (6) can be rewritten as

$$D_{b,eq}=\left(\frac{8\gamma_b}{3k_BT}\right)^{\frac{1}{3}}\left\{\frac{1}{f_{2VP_b}^{\ 2}\left[f_{2VP_b}+f_{PS_b}\left(\frac{a_{PS}}{a_{2VP}}\right)\right]}\right\}^{\frac{1}{3}}a_{2VP}^{\ \frac{5}{3}}N_{2VP_b}^{\ \frac{2}{3}} \quad (7)$$

Equation (7) predicts the well-known $N^{2/3}$ power law of the domain spacing for linear diblock in the strong segregation regime.[23,24]

In the case of EGC, the backbone of the copolymer molecule is composed of the end free blocks constrained by one junction point and the inner blocks constrained by two junction points, as illustrated in Figure 5b. The grafts are attached to the junction points. In the microphase-separated state, the inner blocks may adopt the loop conformation as schematically illustrated in Figure 5b. The looping causes an additional loss of entropy.[25] Because the height of the loop formed by the inner blocks is lower than that of the end block, we assume that a fraction of the end block cover over the top of the loop to maintain uniform segmental density, as shown in Figure 5c. This type of chain arrangement is called "cosurfactant effect," as found in the blends of block copolymers of different molecular weights.[26,27] It is noted that, besides loop conformation, the inner P2VP blocks might also adopt the bridge conformation, where inner blocks serve as the tie chains connecting two adjacent PS microdomains. However, such a bridge conformation allows the arrangement of only a monolayer of P2VP chains in the microdomain and hence prescribes a higher interfacial free energy due to larger surface area, besides the intrinsic entropic loss. As a result, bridge conformation was not considered for the inner blocks of the EGC in our thermodynamic model.

According to Figure 5c, the P2VP lamellar microdomain in the EGC is divided into two sublayers with the thickness of d_{mn} and d_{en}. For one copolymer molecule, the first sublayer is composed of one inner loop block with the mass of m_{2VP_n} and half of the two end blocks. Therefore, we can write

$$n\Sigma_n d_{mn}\rho_{2VP}=(n-1)m_{2VP_n}+\frac{m_{2VP_n}}{2}\times 2 \quad (8)$$

where n is the number of junction points per copolymer molecule. The second sublayer consists of the other half of the end blocks, thus

$$n\Sigma_n d_{en}\rho_{2VP}=\frac{m_{2VP_n}}{2}\times 2 \quad (9)$$

From Equations (8) and (9), we can express the junction point cross sectional area of EGC as

$$\Sigma_n=\frac{m_{2VP_n}}{d_{mn}\rho_{2VP}}=\frac{m_{2VP_n}}{nd_{en}\rho_{2VP}} \quad (10)$$

Consequently, we obtain the relation between d_{mn} and d_{en} as

$$d_{en}=\frac{d_{mn}}{n} \quad (11)$$

For the free energy terms of the EGC, the interfacial free energy per copolymer molecule is given by

$$F_{int}=n\Sigma_n\gamma_n \quad (12)$$

For the conformational entropy, we consider the entropies associated with n PS grafts and one P2VP backbone chain, which is further divided to $(n-1)$ inner block and two free end blocks. The conformational free energy of an EGC molecule is hence given by

$$F_{conf}=(n-1)\times\frac{3}{2}k_BT\frac{d_{mn}^{\ 2}}{N_{2VP_n}a_{2VP}^{\ 2}}+2\times\frac{3}{2}k_BT\left[\frac{\left(\frac{d_{2VP_n}}{2}\right)^2}{N_{2VP_n}a_{2VP}^{\ 2}}\right]+n\times\frac{3}{2}k_BT\left[\frac{\left(\frac{d_{PS_n}}{2}\right)^2}{N_{PS_n}a_{PS}^{\ 2}}\right] \quad (13)$$

The domain spacing, D_n, is given by

$$D_n=\frac{d_{2VP_n}}{f_{2VP_n}}=\frac{d_{PS_n}}{f_{PS_n}}=\frac{2d_n}{f_{2VP_n}} \quad (14)$$

where d_n is the thickness of a monolayer in the P2VP domain, as illustrated in Figure 5c. Substituting Equations (10), (11), and (14) into Equations (12), (13) and expressing the

© 2017 WILEY-VCH Verlag GmbH & Co. KGaA, Weinheim
ADVANCED SCIENCE NEWS
www.advancedsciencenews.com

mass of P2VP block as $m_{2\mathrm{VP}_n} = \rho_{2\mathrm{VP}} N_{2\mathrm{VP}_n} a_{2\mathrm{VP}}^3$, the interfacial free energy and the conformational free energy can be expressed in terms of D_n as

$$F_{\mathrm{int}} = 2(n+1)\left(\frac{N_{2\mathrm{VP}_n} a_{2\mathrm{VP}}^3 \gamma_n}{f_{2\mathrm{VP}_n}}\right)\left(\frac{1}{D_n}\right) \tag{15}$$

$$F_{\mathrm{conf}} = \left\{2(n-1)\left(\frac{n}{n+1}\right)^2 + 1\right\}\left[\frac{3}{4}k_{\mathrm{B}}T\left(\frac{f_{2\mathrm{VP}_n}^2}{N_{2\mathrm{VP}_n} a_{2\mathrm{VP}}^2}\right)D_n^2\right] + \frac{3}{8}nk_{\mathrm{B}}T\left(\frac{f_{\mathrm{PS}_n}^2}{N_{\mathrm{PS}_n} a_{\mathrm{PS}}^2}\right)D_n^2 \tag{16}$$

In addition to these two free energy terms, we also consider the looping free energy of the inner P2VP blocks in the EGC, which is expressed as[25]

$$F_{\mathrm{loop}} = n(n-1)\frac{k_{\mathrm{B}}T}{2}\ln(\pi\chi N_{2\mathrm{VP}}) \tag{17}$$

Subsequently, we sum Equations (15)–(17) to yield the total free energy of EGC, F_{tot}, as

$$F_{\mathrm{tot}} = n(n-1)\frac{k_{\mathrm{B}}T}{2}\ln(\pi\chi N_{2\mathrm{VP}}) + 2(n+1)\left(\frac{N_{2\mathrm{VP}_n} a_{2\mathrm{VP}}^3 \gamma_n}{f_{2\mathrm{VP}_n}}\right)\left(\frac{1}{D_n}\right) + \left\{2(n-1)\left(\frac{n}{n+1}\right)^2 + 1\right\}\left[\frac{3}{4}k_{\mathrm{B}}T\left(\frac{f_{2\mathrm{VP}_n}^2}{N_{2\mathrm{VP}_n} a_{2\mathrm{VP}}^2}\right)D_n^2\right] + \frac{3}{8}nk_{\mathrm{B}}T\left(\frac{f_{\mathrm{PS}_n}^2}{N_{\mathrm{PS}_n} a_{\mathrm{PS}}^2}\right)D_n^2 \tag{18}$$

The equilibrium domain spacing, $D_{n,\mathrm{eq}}$, is obtained via $\left(\frac{\partial F_{\mathrm{tot}}}{\partial D_n}\right)_{D_{n,\mathrm{eq}}} = 0$

Thus,

$$D_{n,\mathrm{eq}} = \left(\frac{2\gamma_n}{3k_{\mathrm{B}}T}\right)^{\frac{1}{3}} \times \left\{\frac{(n+1)N_{2\mathrm{VP}_n} a_{2\mathrm{VP}}^3}{f_{2\mathrm{VP}_n}\left[\left(2(n-1)\left(\frac{n}{n+1}\right)^2 + 1\right)\left(\frac{f_{2\mathrm{VP}_n}^2}{2N_{2\mathrm{VP}_n} a_{2\mathrm{VP}}^2}\right) + n\left(\frac{f_{\mathrm{PS}_n}^2}{4N_{\mathrm{PS}_n} a_{\mathrm{PS}}^2}\right)\right]}\right\}^{\frac{1}{3}} \tag{19}$$

Letting $N_{\mathrm{PS}_n} = N_{2\mathrm{VP}_n}\left(\frac{n+1}{n}\right)\left(\frac{a_{2\mathrm{VP}}}{a_{\mathrm{PS}}}\right)^3\left(\frac{f_{\mathrm{PS}_n}}{f_{2\mathrm{VP}_n}}\right)$,

Equation (19) becomes

$$D_{n,\mathrm{eq}} = \left(\frac{2\gamma_n}{3k_{\mathrm{B}}T}\right)^{\frac{1}{3}} \times \left\{\frac{(n+1)}{f_{2\mathrm{VP}_n}^2\left\{\left[2(n-1)\left(\frac{n}{n+1}\right)^2 + 1\right]\left(\frac{f_{2\mathrm{VP}_n}}{2}\right) + \left(\frac{n^2}{n+1}\right)\left(\frac{f_{\mathrm{PS}_n}}{4}\right)\left(\frac{a_{\mathrm{PS}}}{a_{2\mathrm{VP}}}\right)\right\}}\right\}^{\frac{1}{3}} \times a_{2\mathrm{VP}}^{\frac{5}{3}} N_{2\mathrm{VP}_n}^{\frac{2}{3}} \tag{20}$$

Again, $D_{n,\mathrm{eq}}$ is predicted to vary with $N_{2\mathrm{VP}}^{\frac{2}{3}}$. Now, we attempt to relate $D_{n,\mathrm{eq}}$ to the domain spacing of the corresponding PS-*b*-P2VP, $D_{\mathrm{b,eq}}$. We define the ratios of the numbers of the monomer units in the copolymers as

$$X = \frac{N_{2\mathrm{VP}_n}}{N_{2\mathrm{VP}_\mathrm{b}}} \tag{21}$$

Substituting the Equation (21) into the Equation (20), $D_{n,\mathrm{eq}}$ is rewritten as

$$D_{n,\mathrm{eq}} = \left(\frac{2\gamma_n}{3k_{\mathrm{B}}T}\right)^{\frac{1}{3}} \times \left\{\frac{(n+1)X^2}{f_{2\mathrm{VP}_n}^2\left\{\left[2(n-1)\left(\frac{n}{n+1}\right)^2 + 1\right]\left(\frac{f_{2\mathrm{VP}_n}}{2}\right) + \left(\frac{n^2}{n+1}\right)\left(\frac{f_{\mathrm{PS}_n}}{4}\right)\left(\frac{a_{\mathrm{PS}}}{a_{2\mathrm{VP}}}\right)\right\}}\right\}^{\frac{1}{3}} \times a_{2\mathrm{VP}}^{\frac{5}{3}} N_{2\mathrm{VP}_\mathrm{b}}^{\frac{2}{3}} \tag{22}$$

Assuming $a_{\mathrm{PS}} = a_{2\mathrm{VP}}$ and from the expression of $D_{\mathrm{b},eq}$, in Equation (7), we further reorganize Equation (22) to yield

$$D_{n,\mathrm{eq}} = \left(\frac{\gamma_n}{4\gamma_\mathrm{b}}\right)^{\frac{1}{3}} \times \left\{\frac{(n+1)X^2}{f_{2\mathrm{VP}_n}^2\left\{\left[2(n-1)\left(\frac{n}{n+1}\right)^2 + 1\right]\left(\frac{f_{2\mathrm{VP}_n}}{2}\right) + \left(\frac{n^2}{n+1}\right)\left(\frac{f_{\mathrm{PS}_n}}{4}\right)\right\}}\right\}^{\frac{1}{3}} \times f_{2\mathrm{VP}_\mathrm{b}}^{\frac{2}{3}} D_{\mathrm{b,eq}} \tag{23}$$

which expresses $D_{n,\mathrm{eq}}$, in terms of $D_{\mathrm{b,eq}}$.

For the EGCs studied, the molecular weight of PS graft is approximately the same as that of the P2VP blocks in the backbone. Moreover, the mass densities of the two polymers are similar ($\rho_{\mathrm{PS}} = 1.04$ g cm^{-3}, $\rho_{\mathrm{P2VP}} = 1.1$ g cm^{-3}); therefore, the volume fractions can be expressed as

$$f_{2\mathrm{VP}_n} = \frac{n+1}{2n+1} \tag{24}$$

$$f_{\mathrm{PS}_n} = \frac{n}{2n+1} \tag{25}$$

© 2017 WILEY-VCH Verlag GmbH & Co. KGaA, Weinheim

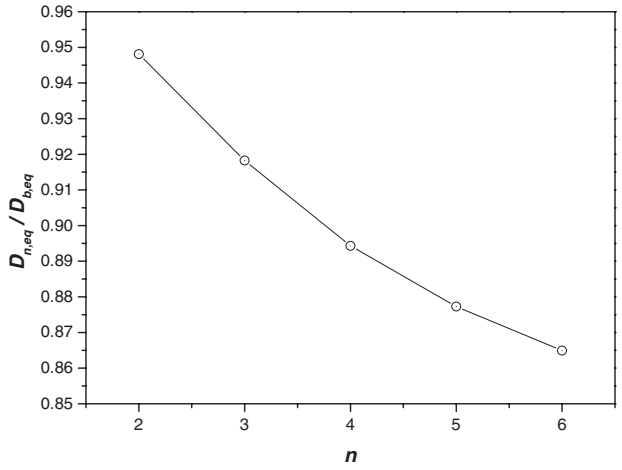

Figure 6. The domain spacing ratio $\frac{D_{n,eq}}{D_{b,eq}}$ of EGC calculated by Equation (26). The calculation assumed $X = 1$ and $\gamma_n = \gamma_b$.

Substituting Equations (24) and (25) into the Equation (23), we obtain the general expression of the domain spacing as

$$D_{n,eq} = \left(\frac{\gamma_n}{\gamma_b}\right)^{\frac{1}{3}}(2n+1)\left\{\frac{X^2}{16\left\{n^2\left[(n-1)+\frac{1}{4}\left(\frac{n}{n+1}\right)\right]+\frac{(n+1)^2}{2}\right\}}\right\}^{\frac{1}{3}} D_{b,eq} \quad (26)$$

According to Equation (26), $D_{n,eq}$ is a complex function of the number of junction point, n. Figure 6 displays the variation of $\frac{D_{n,eq}}{D_{b,eq}}$ with n calculated by Equation (26). The calculation assumed $X = 1$, and $\gamma_n = \gamma_b$. It can be seen that $D_{n,eq}$ decreases progressively with increasing n. This is consistent with our observation that D of EG2 was larger than that of EG3. The calculated ratio $\frac{D_{2,eq}}{D_{3,eq}}$ is 1.089. The observed ratio was 1.057, which agreed very well with the theoretical prediction.

However, the calculated result in Figure 6 predicts $\frac{D_n}{D_b} < 1$, which was inconsistent with the experimental observation showing that the domain spacing of PS-*b*-P2VP was smaller than those of both EG2 and EG3. A previous theoretical work of Olvera de la Cruz and Sanchez has reached the similar conclusion that linear bcp exhibits a larger domain spacing compared to graft copolymer under a given constituent volume fraction.[12] Nevertheless, our experimental results showed opposite trend, that is, $D_{b,eq}$ was smaller than $D_{n,eq}$ of the EGCs.

In the calculation of $\frac{D_{n,eq}}{D_{b,eq}}$ that led to Figure 6, we tacitly assumed $\gamma_n = \gamma_b$, i.e., the surface free energy per unit area of PS-*b*-P2VP was identical to that of the EGC. The surface free energy indeed consists of an enthalpic and entropic part, i.e., $\gamma = \gamma_E + \gamma_S$, where γ_E is prescribed by the interaction energy between PS and P2VP and γ_S is related to the entropy of mixing of S and 2VP monomers in the interface.

Since both PS-*b*-P2VP and the EGCs composed of P2VP and PS blocks, the interaction energy should be the same, i.e., $\gamma_{E,b} = \gamma_{E,n}$. However, γ_S is dependent on the molecular architecture, as schematically illustrated in Figure 7.[28] Each junction point of the linear bcp in the interface is connected with two blocks, whereas that of EGC is connected with three. The stronger junction constraint in EGC decreases the entropy of mixing of the monomers in the interface compared to that associated with the linear diblock. As a result, the surface free energy of EGC should be larger than that of the linear counterpart, that is, the ratio $\frac{\gamma_n}{\gamma_b} > 1$ in Equation (24), which in turn leads to $\frac{D_n}{D_b} > 1$.

3.3. T_{ODT} of the EGC

In addition to the domain spacing, we also found difference in T_{ODT} between the copolymers, where the T_{ODT}

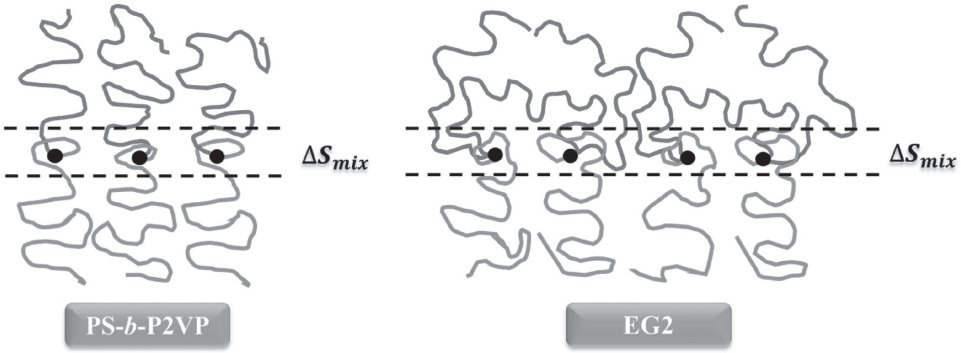

Figure 7. Schematic illustration of the structure of the interface in PS-*b*-P2VP and EG2 to depict that the mixing between 2VP and S monomers in the interface is more constrained by the junction point in EGC.

© 2017 WILEY-VCH Verlag GmbH & Co. KGaA, Weinheim

ADVANCED SCIENCE NEWS
www.advancedsciencenews.com

associated with fluctuation-induced ODT followed the order of: EG3 > EG2 > PS-*b*-P2VP.

The critical point of linear bcp predicted by the mean-field theory of Leiber is $(\chi N)_{ODT} = (\chi N)_{MF} = 10.5$.[2,23] When the effect of fluctuation is considered, the ODT of the symmetric diblock becomes a weak first-order transition; in this case, the fluctuation-induced ODT occurs at a lower critical segregation strength than $(\chi N)_{MF}$. According to the theory of Helfan and Fredrickson, $(\chi N)_{ODT}$ is modified as $(\chi N)_{ODT} = (\chi N)_{MF} + 41\bar{N}^{-1/3}$, where $41\bar{N}^{-1/3}$ is the term arising from the thermal fluctuation effect.[2,20]

According to the mean-field theory of Olvera de la Cruz and Sanchez,[12] the critical segregation strength of ODT of graft copolymer is larger than that of linear bcp under a given volume fraction. Therefore, the T_{ODT} of the linear diblock is expected to be higher than that of the corresponding graft copolymer. In the present study, the ODTs of all copolymers were characterized by a small discontinuity in I_m^{-1} versus T^{-1} plot, attesting that it was a fluctuation-induced transition. Consequently, the critical segregation strength of ODT is prescribed by the inclusion of the fluctuation term. According to the fluctuation theory, the fluctuation effect is depressed as the molecular weight of the copolymer increases; $(\chi N)_{ODT}$ should follow the order of $(\chi N)_{ODT,EG3} < (\chi N)_{ODT,EG2} < (\chi N)_{ODT,PS\text{-}b\text{-}P2VP}$. The T_{ODT} thus followed the order of EG3 > EG2 > PS-*b*-P2VP due to the dominance of the molecular weight effect.

4. Conclusions

We have systematically investigated the phase structure of the EGCs composed of P2VP backbone and PS graft by synchrotron SAXS. T_{ODT} associated with the fluctuation-induced ODT tended to increase with the increase of n, which was attributed to the higher overall molecular weight of the copolymer at larger n. Nevertheless, the domain spacing did not exhibit a monotonic variation with n, as EG2 showed the largest domain spacing compared with EG3 and the corresponding PS-*b*-P2VP diblock copolymer. The experimental observation on domain spacing was explained by formulating the equilibrium domain spacing of graft copolymer assuming that the inner P2VP blocks between the junctions adopted the loop conformation and the two P2VP chains at the ends showed the "co-surfactant" type of packing with the looped chains to attain the normal segmental density in the P2VP microdomain. Our model predicted, decrease of $D_{n,eq}$ with increasing n, and the ratio of $\frac{D_{2,eq}}{D_{3,eq}}$ calculated from the model agreed well with the observed value. However, the model failed to explain the smallest domain spacing displayed by the linear diblock under the assumption of equal surface free energy. We proposed that the free energy of the interface of the EGC is higher than that of the linear diblock due to greater junction constraint that lowers the entropy of mixing of the monomers in the interface. The difference in surface free energy arising from such an entropic effect may cause a smaller domain spacing in the diblock.

Supporting Information

Supporting Information is available from the Wiley Online Library or from the author.

Acknowledgements: This research was supported from the Ministry of Science and Technology, Taiwan, under grant MOST 102-2221-E-007-136-MY3.

Conflict of Interest: The authors declare no conflict of interest.

Received: March 21, 2017; Revised: April 8, 2017; Published online: May 16, 2017; DOI: 10.1002/macp.201700150

Keywords: block copolymer; domain spacing; exact graft copolymer; microphase separation; order–disorder transition

[1] L. Leibler, *Macromolecules* **1980**, *13*, 1602.
[2] F. S. Bates, G. H. Fredrickson, *Annu. Rev. Phys. Chem.* **1990**, *41*, 525.
[3] J. K. Kim, S. Y. Yang, Y. Lee, Y. Kim, *Prog. Polym. Sci.* **2010**, *35*, 1325.
[4] M. W. Matsen, F. S. Bates, *J. Chem. Phys.* **1997**, *106*, 2436.
[5] N. Hadjichristidis, S. Pispas, G. Floudas, *Block Copolymer: Synthetic Strategies, Physical Properties, and Applications*, John Wiley & Sons, Inc., Hoboken, NJ, USA **2003**.
[6] M. W. Matsen, F. S. Bates, *Macromolecules* **1996**, *29*, 1091.
[7] M. W. Matsen, F. S. Bates, *J. Polym. Sci., Part B: Polym. Phys.* **1997**, *35*, 945.
[8] J. K. Kim, J. I. Lee, D. H. Lee, *Macromol. Res.* **2008**, *16*, 267.
[9] M. W. Matsen, *Macromolecules* **2012**, *45*, 2161.
[10] L. Zhang, J. Lin, S. Lin, *J. Phys. Chem. B* **2007**, *111*, 351.
[11] L. Zhang, J. Lin, S. Lin, *J. Phys. Chem. B* **2008**, *112*, 9720.
[12] M. Olvera de la Cruz, I. C. Sanchez, *Macromolecules* **1986**, *19*, 2501.
[13] Y.-T. Chen, C.-T. Lo, *Soft Matter* **2013**, *9*, 1756.
[14] C. Cai, J. Lin, T. Chen, X. Tian, *Langmuir* **2010**, *26*, 2791.
[15] A. Hirao, K. Murano, R. Kurokawa, T. Watanabe, K. Sugiyama, *Macromolecules* **2009**, *42*, 7820.
[16] A. Hirao, M. Uematsu, R. Kurokawa, T. Ishizone, *Macromolecules* **2011**, *44*, 5638.
[17] A. Hirao, K. Murao, A. Abouelmagd, M. Uematsu, S. Ito, R. Goseki, T. Ishizone, *Macromolecules* **2011**, *44*, 3302.
[18] S. Paraskeva, N. Hadjichristidis, *J. Polym. Sci., Part A: Polym. Chem.* **2000**, *38*, 931.
[19] R. J. Roe, *Methods of X-Ray and Neutron Scattering in Polymer Science*, Oxford University Press, New York **2000**.

© 2017 WILEY-VCH Verlag GmbH & Co. KGaA, Weinheim

[20] F. S. Bates, J. H. Rosedale, G. H. Fredrickson, *J. Chem. Phys.* **1990**, *92*, 6255.
[21] G. H. Fredrickson, E. Helfand, *J. Chem. Phys.* **1987**, *87*, 697.
[22] T. T. Koga, T. Hashimoto, *J. Chem. Phys.* **1999**, *110*, 11076.
[23] T. Hashimoto, M. Shibayama, H. Kawai, *Macromolecules* **1980**, *13*, 1237.
[24] T. Hashimoto, M. Fujimura, H. Kawai, *Macromolecules* **1980**, *13*, 1660.
[25] N. P. Balsara, M. Tirrell, T. P. Lodge, *Macromolecules* **1991**, *24*, 1975.
[26] T. Hashimoto, D. Yamaguchi, F. Court, *Macromol. Symp.* **2003**, *195*, 191.
[27] D. Yamaguchi, J. Bodycomb, S. Koizumi, T. Hashimoto, *Macromolecules* **1999**, *32*, 5884.
[28] T. Hashimoto, K. Kowsaka, M. Shibayama, H. Kawail, *Macromolecules* **1986**, *19*, 754.

© 2017 WILEY-VCH Verlag GmbH & Co. KGaA, Weinheim

ADVANCED SCIENCE NEWS
www.advancedsciencenews.com